A model of nitric oxide in the lower thermosphere

Scott M. Bailey
Geophysical Institute, University of Alaska, Fairbanks, Alaska, USA

Charles A. Barth
Laboratory for Atmospheric and Space Physics, University of Colorado, Boulder, Colorado, USA

Stanley C. Solomon
High Altitude Observatory, National Center for Atmospheric Research, Boulder, Colorado, USA

Received 8 August 2001; revised 2 January 2002; accepted 2 January 2002; published XX Month 2002.

[1] A model of NO abundance in the lower thermosphere is described. The model includes time dependence, an energetic electron flux calculation that includes transport, neutral and ion photochemistry, and vertical diffusion. We show that a steady state calculation is inadequate for calculating NO abundance. We examine the relationship between observed NO abundance and the integrated energy input to the lower thermosphere over the previous day. It is shown that the relationship between the energy input and the NO abundance varies with the local time of the NO measurement and with the length of daylight. These dependencies arise due to the role of photodissociation as a loss mechanism for NO. This model is designed for analysis of NO observations and will be used in the analysis of observations by the SNOE spacecraft [*Barth et al.*, 1999]. *INDEX TERMS:* 0355 Atmospheric Composition and Structure: Thermosphere—composition and chemistry; 0358 Atmospheric Composition and Structure: Thermosphere—energy deposition; *KEYWORDS:* thermosphere, nitric oxide, model, photoelectrons, aurora

1. Introduction

[2] The importance of nitric oxide in the lower thermosphere has long been recognized. Due to its unique properties, NO plays an important role in the structure and energetics of the upper atmosphere. Because it has a low ionization threshold, the NO density controls the ion composition of the *E* region of the ionosphere, and photoionization of NO by the solar Lyman-α emission creates the *D* region. NO is a heteronuclear molecule and therefore emits efficiently in the infrared, which is an important source of radiational cooling in the thermosphere. Thus NO plays an important role in the thermospheric energy balance and temperature structure. If transported to lower altitudes, as is likely in the polar regions during winter, NO will catalytically destroy ozone.

[3] The sources of production and loss of NO have been brought to light over the last four decades by numerical modeling and comparisons with many sounding rocket and several satellite experiments. Satellite experiments such as the Solar Mesosphere Explorer (SME) [*Barth et al.*, 1988] and the Halogen Occultation Experiment (HALOE) [*Russell et al.*, 1993] have shown that thermospheric NO is highly variable in both space and time with abundances varying by an order of magnitude. These experiments have also shown that the NO abundance is strongly related to the solar irradiance and auroral conditions [*Barth et al.*, 1988; *Siskind et al.*, 1990]. The peak in thermospheric NO abundance occurs near 106 km. At low latitudes, NO has typical abundance of about 100×10^{12} m^{-3} and can vary from about half of that value to twice that value. The solar soft X-ray irradiance is the primary energy driver for producing NO at these latitudes [*Barth et al.*, 1988, 1999]. At high latitudes, auroral energy is the primary energy source [*Rusch and Barth*, 1975; *Solomon et al.*, 1999] and the variability is even larger with the magnitude typically at least twice that of the lower latitude abundance.

[4] The abundance of NO is a key indicator of energy deposition to the upper atmosphere. NO is primarily produced through the reaction of excited atomic nitrogen with molecular oxygen. In order to produce the excited atomic nitrogen atom, the strong N_2 molecular bond must be broken. At high latitudes, auroral electrons and energetic secondary electrons provide the source of energy that leads to the large amounts of NO which are observed. Globally, solar soft X-rays are a source of energy that leads to the production of NO. It stands to reason then, that a measurement of the abundance of thermospheric NO, is an indicator of solar energy deposition into the upper atmosphere. The Student Nitric Oxide Explorer (SNOE) satellite was launched on February 27th, 1998 [*Barth et al.*, 1999; *Solomon et al.*, 1999; *Bailey et al.*, 1999]. This experiment, which has been in operation for over three years, measures NO and solar soft X-rays simultaneously during a time when auroral energy deposition is also measured by several experiments that are part of the International Solar Terrestrial Physics Program. Analyzing the SNOE NO measurements along with the solar soft X-ray measurements and the auroral energy input allows the first quanti-

0148-0227/02/2001JA000258$09.00

tative studies of the utility of NO as a diagnostic of solar energy input.

[5] The goal of this paper is to develop and describe the numerical model that will be used to analyze the SNOE data. In an upcoming companion paper, we will compare the SNOE observations to predictions from the model. The model we present here is a new development over previous time-dependent models of NO in that it incorporates a treatment of energetic electron transport at each time step. Including electron transport improves the accuracy of the calculations over previous versions of this model because it removes the need to make the local approximation for photoelectrons and because parameterizations of auroral ionization rates are no longer used. Since the primary objectives of the SNOE mission are to understand the relationship between NO abundances and the sources of energy that lead to its production, this model is an appropriate new tool for that task. The following section will describe the theory of NO. Section 3 will describe the calculation of N_2 ionization and dissociation by energetic electrons. Sections 4 and 5 will describe steady state and time-dependent numerical calculations of NO abundances. Section 6 will discuss the relationship between NO measurements and energy deposition to the atmosphere.

2. Theory of Nitric Oxide

[6] Nitric oxide in the upper atmosphere is produced in the reaction between atomic nitrogen and molecular oxygen,

(R1) $$N(^4S) + O_2 \rightarrow NO + O.$$

[7] This reaction is strongly dependent upon temperature. While this reaction with ground state atomic nitrogen dominates the production of NO at higher altitudes, excited atomic nitrogen reacting with molecular oxygen provides the primary production of NO at the peak altitudes,

(R2) $$N(^2D) + O_2 \rightarrow NO + O.$$

[8] Reactions with ground state atomic nitrogen and O_2^+ provide loss mechanisms for NO,

(R3) $$NO + N(^4S) \rightarrow N_2 + O,$$

(R4) $$NO + O_2^+ \rightarrow NO^+ + O_2.$$

[9] In addition, during the daytime, photodissociation by solar ultraviolet irradiance also provides a loss process for NO,

(R5) $$NO + h\upsilon \rightarrow N(^4S) + O.$$

[10] Note that only reaction R3 truly destroys Odd-N (molecules with an odd number of N atoms). Reactions R4 and R5, while destroying NO, only recycle the Odd-N. However, the destruction of NO through photodissociation, reaction R5, produces a ground state nitrogen atom which can in turn also destroy NO and thus enhance the effectiveness of the photodissociation for destroying NO and removing Odd-N. *Barth* [1992] compared the strengths of photodissociation and reactions with ground state nitrogen atoms as loss mechanisms for NO.

[11] The key to producing NO is in breaking the strong N_2 bond and producing an excited nitrogen atom. There are several methods for producing $N(^2D)$. One significant method is dissociative recombination of NO^+,

(R6) $$NO^+ + e \rightarrow N(^2D, ^4S) + O,$$

or similarly dissociative recombination of N_2^+,

(R7) $$N_2^+ + e \rightarrow 2N(^2D, ^4S).$$

[12] Both of the above reactions occur with ambient electrons. Another important production of $N(^2D)$ is through energetic electrons,

(R8) $$N_2 + e^* \rightarrow 2N(^2D, ^4S) + e^*.$$

[13] This process requires about 10 eV of electron energy to accomplish. At high latitudes, these energetic electrons are precipitating auroral electrons and secondary electrons. At lower latitudes these energetic electrons are produced through photoionization processes and are referred to as photoelectrons. Another way energetic electrons lead to $N(^2D)$ production is through a two step process whereby the N_2 molecule is first ionized and the N_2 ion then reacts with O,

(R9) $$N_2 + e^* \rightarrow N_2^+ + e + e^*, \text{ and}$$

(R10) $$N_2^+ + O \rightarrow NO^+ + N(^2D).$$

[14] The production and loss of NO clearly depends on the relative amounts of excited and ground state atomic nitrogen. More fundamentally, the abundance of NO depends critically on the solar illumination. Excited atomic nitrogen which is required to produce NO as well as ground state atomic nitrogen and O_2^+ which destroy NO are all created through processes involving solar irradiance. In addition the solar UV irradiance can directly destroy NO. Thus, when the atmosphere is illuminated by the Sun, photoelectrons are produced and lead to the production of excited atomic nitrogen which in turn reacts with O_2 to form NO. Photoelectrons also produce ground state nitrogen, which then destroys the NO, as does O_2^+ created through photoelectron ionization and direct photoionization. At night, with the exception of auroral production, any remaining ground state nitrogen and O_2^+ will reduce the amount of NO. Some NO is created as excited atomic nitrogen is created from the reaction between NO^+ and any remaining ambient electrons. This NO production will not last long as there is no production of ground state atomic nitrogen, O_2^+, or ambient electrons to sustain them. As the loss processes are removed, significant amounts of NO may begin to be transported lower in altitude. Thus at some altitudes, the abundance of NO may decrease, while at some lower altitudes, the NO abundance may increase. Auroral precipitation will strengthen the production of NO and leads to higher NO abundances in the auroral region. The auroral production is very efficient at night because although the

aurora does produce ground state atomic nitrogen and O_2^+, there is no photodissociation.

[15] The lifetime of an NO molecule to chemical destruction (or e-folding time in the NO density) under illuminated conditions is 19 hours [*Barth et al.*, 2001]. The lifetime of the NO molecule to diffusive transport is approximately one day [*Barth*, 1992]. Given that the solar illumination varies throughout the day, the abundance of NO at any one time is then representative of the level of solar energy deposition (solar irradiance and auroral energy) over the past day.

[16] The above discussion describes the most important processes for producing and destroying NO and shows that the key to understanding NO lies in understanding the energy deposition into the atmosphere that leads to its production. Section 4 provides more detail into the chemistry of NO. In the next section we describe a theory for calculating the transport of energetic electrons through the atmosphere and calculation of the ionization and dissociation they produce. In the following sections we then describe a steady state and then a time dependant model for calculating the altitude distribution of NO based on the ionization and dissociation rate profiles.

3. Calculation of Energetic Electron Impact Ionization and Dissociation

[17] The importance of photoelectrons in the atmosphere was first suggested by *Hanson and Johnson* [1961]. *Barth* [1969] pointed out the utility of photoelectron impact excited emissions in the remote sensing of planetary atmospheres and described the necessary physics for interpreting the brightnesses of those emissions. Numerical modeling of photoelectron fluxes for calculating emission rates has progressed for nearly three decades. Early works include that by *Dalgarno et al.* [1963], *Green and Barth* [1967] and *Dalgarno et al.* [1969]. Because calculations were computationally intensive, parameterizations were introduced [*Stewart*, 1970]. As computers became faster and more available, numerical techniques were developed. Monte Carlo methods were employed [*Cicerone and Bowhill*, 1971] and the equation of transfer was solved using two stream [*Nagy and Banks*, 1970; *Stamnes*, 1981a, 1981b] and multistream methods [*Strickland et al.*, 1976; *Oran and Strickland*, 1978; *Link*, 1982]. Rapid calculation of photoelectron excitation rates was performed assuming the local approximation [*Strickland and Meier*, 1982]. *Cicerone et al.* [1973] compared the application of several methods of photoelectron fluxes and found good agreement at altitudes where the local approximation applied. In the current era, computers are fast enough that photoelectron spectra and excitation rates can be computed rapidly without making the local approximation. Models using the above numerical techniques are described by *Solomon et al.* [1988], *Richards and Torr* [1990], *Link* [1992], and references therein. Today, the numerical methods employed are relatively mature; any discrepancies among the various models are probably due to differences in the cross sections employed. For this work, the glow model [*Solomon et al.*, 1988; *Solomon and Abreu*, 1989] will be used to calculate the photoelectron spectrum. The model follows a two-stream formalism and includes electron transport.

[18] The glow model is a comprehensive set of numerical routines that calculate energetic electron fluxes in the atmosphere and use them to derive profiles for a variety of atmospheric observables. The computer code is available as collaborative software. The method of calculation follows that described by *Nagy and Banks* [1970].

[19] The energetic electron flux calculation follows a two-stream formalism. The basic premise of such a method is the assumption that the angular dependence of the problem can be simplified by performing calculations in two directions along a single path. The ''two-stream'' name comes from the fact that calculations must be made in both the upward and downward directions. Because electrons travel along Earth's magnetic field in a spiral motion, it is logical that the path of travel used here be at a representative pitch angle to the magnetic field. In the glow model, the path is along a pitch angle of 60°, more commonly referred to by its cosine of 0.5.

[20] For the problem at hand we consider an atmosphere of molecular nitrogen (N_2), atomic and molecular oxygen (O and O_2), and nitric oxide (NO). Solar soft X-ray and EUV irradiance ionize these gases creating energetic photoelectrons. These electrons can cause further ionization or excitation by impact with other atoms or molecules. The initial ionization by a solar photon results in a primary photoelectron. Photoelectrons created through ionization by other photoelectrons are called secondary photoelectrons. In an aurora, the deposition of energetic electrons into the atmosphere is a source of energy in addition to the solar irradiance. The precipitating primary electrons are modeled with an energy spectrum; the energetic electrons remaining after energetic electrons collide and interact with atmospheric particles are secondary electrons. The glow model can handle both photoelectrons and auroral electrons simultaneously.

[21] In the two-stream formalism, the solar irradiance incident upon the atmosphere at some solar zenith angle is considered. A neutral atmosphere varying only with altitude is assumed and a slant path from the top of the atmosphere is followed. Along the path, electrons can be scattered forwards or backwards by elastic collisions or they can undergo an inelastic collision resulting in ionization, dissociation, or excitation. The sum of these processes will be labeled T_2. Electrons undergoing elastic collisions are labeled T_1. Both T_1 and T_2 are functions of altitude, and have units of cm^{-1} corresponding to production or loss per unit length. The following forms are used:

$$T_1 = \sum_s b_s \sigma_s^{es} n_s, \tag{E-1}$$

$$T_2 = \sum_s \left(b_s \sigma_s^{es} n_s + \sigma_s^{is} n_s\right) \tag{E-2}$$

where n is the number density of scattering atoms or molecules, b is the backscatter probability, and σ^{es} and σ^{is} are the elastic and inelastic cross sections respectively. The subscript s stands for atmospheric species. For a two-stream case, the backscatter probability is the probability of reversing directions after an elastic collision. In each energy bin, primary photoelectron production q and cascade from higher energy photoelectrons in either stream undergoing elastic or inelastic collisions Q are accounted for. Both Q and q have units of $cm^{-3}\ s^{-1}$. Defining μ as the cosine of the angle between the path and the magnetic field (i.e. the

cosine of the characteristic pitch angle), ϕ as the flux of photoelectrons ($cm^{-2}\ s^{-1}$, a function of electron energy and altitude), + and − superscripts as the upward and downward directions, and z as the distance along the field line, the two-stream equations of electron transport are:

$$\mu\frac{d\phi^+}{dz} = -T_2\phi^+ + T_1\phi^- + Q^+ + \frac{q}{2}, \quad \text{(E-3)}$$

$$-\mu\frac{d\phi^-}{dz} = -T_2\phi^- + T_1\phi^+ + Q^- + \frac{q}{2}. \quad \text{(E-4)}$$

[22] Taking the derivative of equation E-4, substituting E-3 and solving gives the following results:

$$\frac{d^2\phi^-}{dz^2} + \alpha\frac{d\phi^-}{dz} + \beta\phi^- + \gamma = 0. \quad \text{(E-5)}$$

[23] Here α, β, and γ are collected terms in T_1, T_2, q, Q, and their spatial derivatives,

$$\alpha = -\frac{1}{\mu}\left(2T_2 + \frac{\mu}{T_1}\frac{dT_1}{dz}\right), \quad \text{(E-5)}$$

$$\beta = \frac{1}{\mu}\left(\frac{T_1^2}{\mu} + \frac{T_2^2}{\mu} + \frac{T_2}{T_1}\frac{dT_1}{dz} - \frac{dT_2}{dz}\right), \quad \text{(E-6)}$$

$$\gamma = \frac{1}{\mu}\left[\frac{T_1Q^+}{\mu} - \frac{T_2Q^-}{\mu}\right] + (T_1 - T_2)\frac{q}{2\mu} - \left(Q^- + \frac{q}{2}\right)\frac{1}{T_1}\frac{dT_1}{dz} + \frac{dQ^-}{dz} + \frac{1}{2}\frac{dq}{dz}.$$

[24] Equation E-5 is a second order ordinary differential equation. In the glow model, the equation for ϕ^- is solved using the steady state Crank-Nicholson numerical technique. This method is generally applicable to parabolic partial differential equations, using an iterative approach. For the steady state case at hand, a solution can be obtained in one iteration. A complete description is given by *Von Rosenberg* [1969]. Once ϕ^- has been calculated at all altitudes, ϕ^+ is obtained from E-4 from the lower boundary to the upper. Two boundary conditions are required to obtain a solution. At the top of the atmosphere, the downward flux is a given value appropriate for the particular problem. In the case of an aurora, a primary spectrum of energetic electrons is used. Although any spectrum can be accommodated, a Maxwellian distribution with a given characteristic energy and integrated energy flux is typically assumed. In the non-auroral case, the downward flux is set to zero, which assumes that the conjugate flux (that flux following the field line from the opposite hemisphere) is neglected. At the lower boundary, the downward flux must equal the upward flux. The lower boundary is set low enough in altitude that both fluxes are very near zero at all energies.

[25] The solar irradiance data required for these calculations range in wavelength from the EUV downward to the soft X-ray region of the spectrum, the entire ionizing region of the solar spectrum. The solar spectrum in the glow model is incorporated in 1 nm wavelength intervals. Previous works using the glow model have used solar fluxes from empirical models and past measurements [*Hinteregger et al.*, 1981; *Woods and Rottman*, 1990; *Tobiska*, 1991]. In the current utilization, the EUV irradiance model of *Hinteregger et al.* [1981] is used longward of 20 nm. Below 20 nm, the solar minimum spectrum of *Hinteregger et al.* [1981] is scaled by three scaling factors for three wavelength intervals, 2–7 nm, 7–17 nm, and 17–20 nm, which are input parameters. These three bandpasses are chosen because they are the SNOE Solar Soft X-ray Photometer bandpasses [*Bailey et al.*, 1999, 2001].

[26] For a typical run of the glow model, a model atmosphere is obtained from two sources. Profiles for the neutral species and temperatures are obtained from the Mass Spectrometer Incoherent Scatter model (MSIS) [*Hedin*, 1987]. Initial electron and ion densities and temperatures are obtained from the International Reference Ionosphere [*Belitza*, 1986] although the glow model will calculate these values at the altitudes relevant to NO. Measured atmospheric profiles can also be accommodated. In order to calculate the rates of elastic and inelastic collisions, the glow model incorporates a large body of electron impact cross section data. Appendix 1 of *Solomon et al.* [1988] details the many electron impact cross sections used. The photoabsorption cross sections are those of *Fennelly and Torr* [1992]. Branching ratios for the various possible results of each photoabsorption are taken from *Conway* [1988].

[27] An important contribution to the photoionization term of equation E-2 is due to Auger electrons. The effects of Auger ionization were first calculated by *Avakyan et al.* [1977]. The first measurements to demonstrate their importance were from the Dynamics Explorer 2 satellite [*Winningham et al.*, 1989]. A detailed description of Auger processes is given by *Berkowitz* [1979]. The process of Auger ionization occurs when the impinging photon has enough energy to remove a K-shell electron from the atom or molecule with which it collides. Since the removal of the inner electron takes a great deal of energy (360 eV for N_2), the electron produced typically has very little energy. The interesting aspect of Auger ionization, however, is what occurs after the K-shell electron is released. The vacancy in the K-shell is immediately filled, so an outer shell electron takes its place. In doing so, the atom gives up the same amount of energy that was required to break free the K-shell electron. This energy is released with another outer shell electron. For molecules comprised of elements with atomic numbers less than 20, this process also dissociates the molecule [*Berkowitz*, 1979]. The Auger process is written symbolically for N_2 in the following way:

$$N_2 + h\upsilon(>400eV) \rightarrow N + N^{++} + e(400eV - 25.8eV) + e(h\upsilon - 400eV). \quad \text{(E-8)}$$

[28] The 25.8 energy in equation E-8 is the 10 eV needed to dissociate the molecule and the 15.8 eV needed to remove the outer shell electron. The process is similar for O_2 and O, except there is no dissociation involved with atomic oxygen. Auger ionization is incorporated into the glow model as described above.

[29] Figure 1 shows examples of photoelectron spectra calculated at 150 and 106 km. These spectra were calculated for the geophysical conditions of day 266, fall equinox, of 1999. The location is the equator at 0° longitude and a local time of 11AM. For each of the three soft X-ray bandpasses, an energy flux of 1 mW m^{-2} is assumed. The general trend

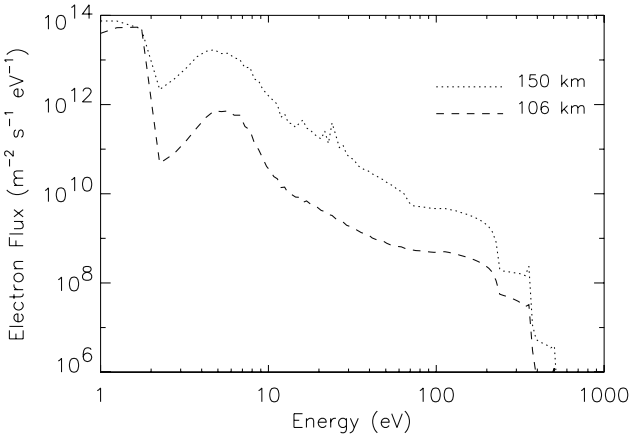

Figure 1. Energetic electron fluxes at 150 km and 106 km produced by solar irradiance as calculated by the glow model. Shown is the sum of upward and downward electron fluxes. The geophysical conditions for this calculation are appropriate to day 266 of 1999. The latitude is 0° and the longitude is 0°. The local time is 11:00AM and the solar soft X-ray energy flux is 1 mW m^{-2}.

in Figure 1 is increasing photoelectron fluxes toward lower electron energies. This is because the photoelectrons tend to cascade toward lower energies as they collide with the atmospheric constituents. Each collision leads to an ionization, dissociation, or excitation of that species, which reduces the energy of the electron. Therefore, as each electron eventually transfers its energy to the atmosphere, any snapshot of the photoelectron spectrum shows only a few high-energy electrons and increasing numbers of electrons toward the lowest energies as they transfer their energy to the atmosphere. Below 3 eV, a dip appears in the photoelectron spectrum, this dip is due to vibrational excitation of N_2 for which there is a large cross section at these energies. Model calculations of photoelectron spectra using SNOE solar irradiances have been compared to measured photoelectron fluxes by *Solomon et al.* [2001]. The model was shown to reproduce the data very well.

[30] Some peaks also occur in the photoelectron spectra, especially at 150 km. The most obvious are at 25 and 335 eV. The feature at 25 eV is due to the very bright solar He II emission at 30.4 nm. This feature is nearly an order of magnitude brighter than the emissions surrounding it in the solar spectrum. The energy of a 30.4 nm photon is about 40 eV; the ionization energy of O or N_2 is about 15 eV. Therefore, we expect a peak near 25 eV. The peak at 335 eV is due to Auger ionization of N_2.

[31] For the auroral case, Figure 2 shows the energetic electron fluxes at 150 and 106 km. Shown with the spectra at these altitudes is the original Maxwellian input spectrum. The input spectrum has an integrated energy flux of 1 mW m^{-2} and a characteristic energy of 4 keV. The geophysical conditions are again for day 266 of 1999 and the location is now 65° latitude, 0° longitude. No solar soft X-ray irradiance is included in this calculation. In this auroral case, the spectra are much smoother than the photoelectron case, reflecting the smoothness of the input spectrum. The general increase in flux with decreasing energy and the dip at low energies are still seen for the same reasons as above.

[32] Once the energetic electron spectrum is found at each altitude, ionization, dissociation, or excitation rates by electron impact can be calculated by the following integration:

$$\int_0^\infty \phi(E,z)\sigma(E)n_s(z)dE. \qquad \text{(E-7)}$$

[33] Here ϕ is the photoelectron flux, σ is the cross section for the process under consideration, E is electron energy, and n_s is the number density of the atmospheric species undergoing the process.

[34] Figure 3 shows the results of O, O_2, and N_2 ionization and N_2 dissociation by solar irradiance produced photoelectrons from the calculation that was used to produce Figure 1. For this case, the peak is located at about 110 km. The peak can be located as high as 150 km and a double peak may occur depending on the relative strengths of the solar soft X-ray and the 30.4 nm irradiances. Figure 4 shows N_2 ionization rate profiles for the same case as Figure 2 but for characteristic energies of 1, 2, 3, 4, 5, and 6 keV. Each profile assumes an integrated energy flux of 1 mW m^{-2}. Increasingly higher characteristic energies clearly produce peak ionization at increasingly lower altitudes. Electron spectra with characteristic energies between 3 and 6 keV deposit their energy near 106 km.

4. Steady State Calculation of Nitric Oxide Densities

[35] Once a calculation of the energetic electron fluxes is performed, the actual NO densities can be calculated using the theory of section 2. We point out that while the primary components to the theory of NO were described in

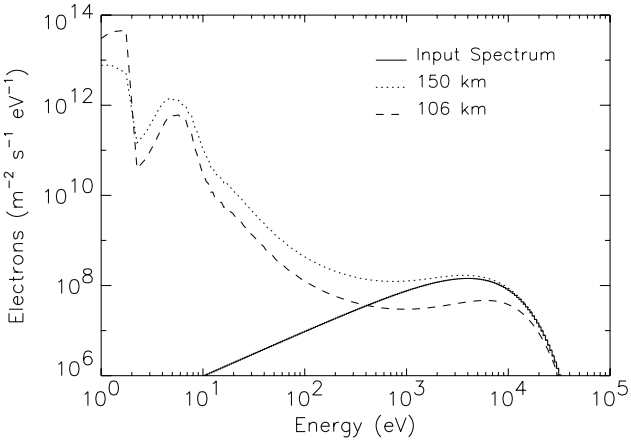

Figure 2. Energetic electron fluxes at 150 km and 106 km produced by auroral electrons as calculated by the glow model for auroral conditions. Shown is the sum of upward and downward electron fluxes. Also shown by the solid line is the input auroral energetic electron spectrum. The geophysical conditions for this calculation are appropriate to day 266 of 1999. The latitude is 65°N and the longitude is 0°. The local time is 11:00AM. The characteristic energy of the auroral electron spectrum is 4 keV and the integrated energy flux is 1 mW m^{-2}.

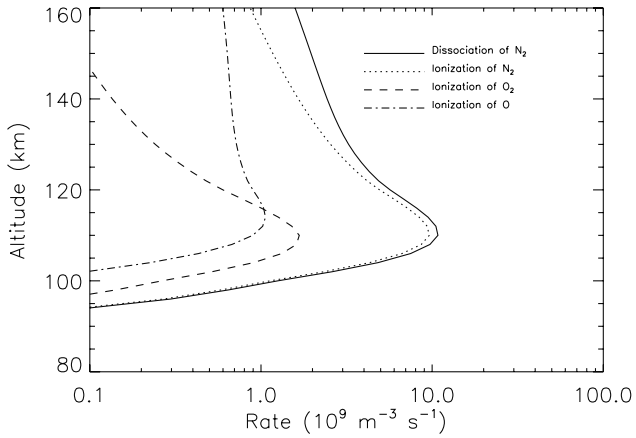

Figure 3. Ionization rates of N_2, O_2, and O and the dissociation rate of N_2 by solar irradiance produced photoelectrons as calculated by the glow model. Geophysical conditions and energetic inputs are the same as Figure 1.

section 2, there are other reactions that must be considered in order to form a closed system. *Barth* [1992] lists all of the relevant reactions and their rate coefficients. A tabulation of the rate coefficients for those chemical reactions listed in this work and those for which the rate coefficients have been updated since *Barth* [1992] is presented in Appendix A. The NOx 1-D model calculates NO profiles for given geophysical conditions. The term 1-D indicates that the model is one-dimensional: vertical transport of atmospheric constituents is accounted for, but horizontal transport and time dependence are neglected. Earlier versions of this model have been described by *Cleary* [1986], *Siskind et al.* [1989a, 1989b, 1990, 1995], *Eparvier* [1991], and *Barth* [1992]. The present model is an improvement over the previous versions in that several key reaction rate coefficients have been updated (see Appendix A) and most importantly because the glow energetic electron flux calculation has been included. The incorporation of the glow model improves accuracy because it removes the need for the local approximation in photoelectron calculations and includes all of the relevant solar photon energies. Both of these effects are described below. Previous versions of the NO model used parameterizations for the auoroal ionization rates. Incorporating the glow model removes the need for these parameterizations. *Swaminathan et al.* [1998] has also presented NO model results with a similar compilation of rate coefficients and atmospheric parameters.

[36] To solve for the density of an atmospheric constituent, the one-dimensional mass continuity equation is solved neglecting horizontal transport:

$$\frac{\partial n_s}{\partial t} = P_s - L_s n_s - \frac{\partial \Phi_s}{\partial z}, \tag{E-9}$$

where n_s is the number density of species s, P_s is the production rate of species s (cm^{-3} s^{-1}), L_s is the loss rate of species s (s^{-1}), and Φ_s is the vertical flux of the species s (cm^{-2} s^{-1}). This equation simply states that the rate of change of a given species, namely NO, is the difference between the production and loss of that species minus the amount of that species which is transported to another altitude. The production and loss rates are due primarily to the processes described in section 2.

[37] The vertical flux Φ_s can be written as,

$$\Phi_s = -D_s\left(\frac{\partial n_s}{\partial z} + \frac{n_s}{T}\frac{\partial T}{\partial z} + \frac{n_s}{H_s}\right) - K\left(\frac{\partial n_s}{\partial z} + \frac{n_s}{T}\frac{\partial T}{\partial z} + \frac{n_s}{H}\right), \tag{E-10}$$

where D_s is molecular diffusion coefficient, K is the Eddy diffusion coefficient, T is temperature, H_s is the scale height for species s while H is the mean atmospheric scale height [*Colegrove et al.*, 1965]. Equation E-10 can be differentiated and substituted into E-9 to produce,

$$\frac{\partial n_s}{\partial t} = A_s\frac{\partial^2 n_s}{\partial^2 z} + B_s\frac{\partial n_s}{\partial z} + Cn_s + E_s, \tag{E-11}$$

where A_s, B_s, C_s, and E_s are collected terms in D, K, P, L,T, and H.

[38] Equation E-11 is a second order ordinary differential equation like E-6 and can be discretized and solved with the same Crank-Nickolson algorithm [*Von Rosenberg*, 1969] as E-6. This process is done for both NO and N(^{4}S) as diffusion is important for these constituents. For N_2^+, N^+, O_2^+, O^+, O^+(2D) , NO^+, and N(^{2}D), chemical processes occur much more quickly than diffusive processes, they are in chemical equilibrium; therefore, the last term in equation E-9 can be ignored, simplifying the solution. The boundary conditions used in the solution of NO and N(^{4}S) are that at the highest altitude (200 km) there is no upward flux of either species. At the lowest altitude (70 km) NO is assumed to be at a minimum and N(^{4}S) is assumed to be in photochemical equilibrium.

[39] The model begins with the profiles of all minor species having zero values, the major species coming from the MSIS model, and the ionization and dissociation rates coming from the glow model. Equation E-11 (or E-9) is solved and the minor species values are updated. The process is repeated until convergence occurs. Experience

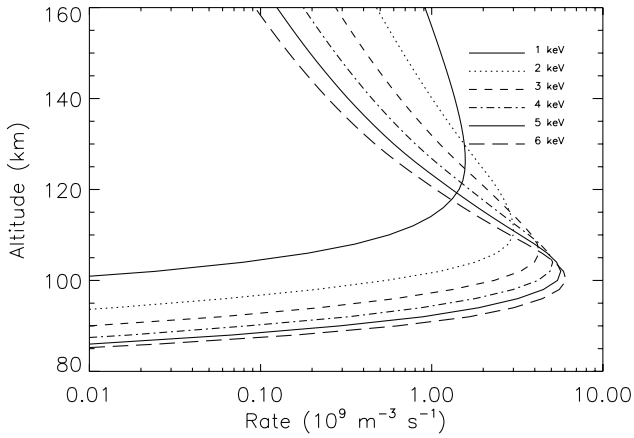

Figure 4. Ionization rates of N_2 for auroral electrons of different characteristic energies as calculated by the glow model. Geophysical conditions and energetic inputs are the same as for Figure 2.

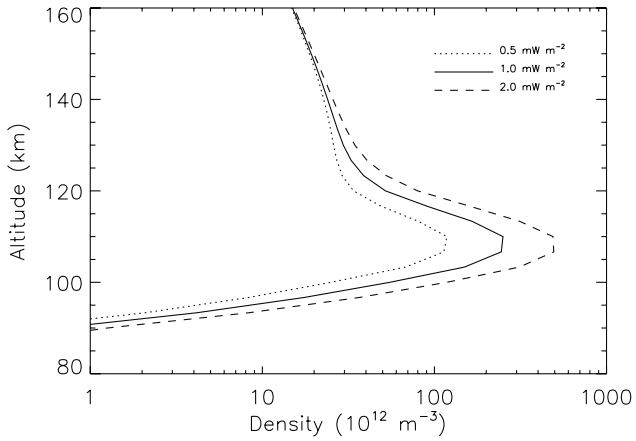

Figure 5. Nitric oxide densities as a function of altitude produced by solar irradiance photoelectrons as calculated by the combined glow and NOx models. Geophysical conditions are the same as in Figures 1 and 3. The model is run for 2–7 nm solar irradiances of 0.5, 1.0, and 2.0 mW m^{-2}.

has shown that running the model for 120 hours with time steps of 900 s (later increasing to 3600 s) is sufficient to achieve convergence. Because this calculation is steady state, none of the geophysical conditions or energetic inputs are allowed to change during the calculation. This model is then representative of equilibrium NO produced under constant conditions.

[40] Figure 5 shows the results of the steady state calculation for the case of solar irradiance (photoelectron) produced NO. Shown are altitude profiles of NO density for the conditions of Figures 1 and 3 with 2–7 nm solar soft X-ray energy fluxes of 0.5, 1.0, and 2.0 mW m^{-2}. These values represent low, medium, and high-energy fluxes based upon the SNOE measurements [*Bailey et al.*, 2001]. The peaks in the NO profile are consistently seen at about 106 km. At this altitude and for the photoelectron case, a doubling of energy input results in approximately a doubling of NO density. At lower and higher altitudes, the effect of doubling the solar soft X-ray irradiance is smaller as these altitudes are primarily dependant upon higher and lower energy solar photons. *Barth* [1992] shows a model calculation for similar levels of solar activity. The results in Figure 5 are more than a factor of two larger than those model predictions. The discrepancy is explained by the incorporation of the glow photoelectron flux calculation. *Barth* [1992] used the photoelectron model of *Strickland and Meier* [1982]. The Strickland and Meier model is a local calculation and ignores photoelectron transport. The version of the Strickland and Meier model used ignored solar photons below 7 nm except for 18 solar emission lines between 2 and 5 nm. A scale factor for the brightness of the 18 lines was a free parameter in the model. The glow model includes electron transport and the full solar spectrum down to 1.8 nm. These changes result in the production of more ionization and dissociation than the previous model. Half of the energy in the solar spectrum between 2 and 7 nm lies in the 5 to 7 nm range; thus, the factor of two difference between *Barth* [1992] and Figure 5 is due to the missing solar irradiance. *Siskind et al.* [1995] discuss the importance of including a modern photoelectron flux calculation.

[41] Figure 6 shows the results of the steady state calculation for the case of auroral energy deposition shown in Figures 2 and 4. Calculations for characteristic energies of 1, 2, 3, 4, 5, and 6 keV are shown. These values cover a nominal range in auroral characteristic energies. In each case an integrated energy flux of 1 mW m^{-2}, which is a frequently occurring but low energy flux, is assumed. Higher characteristic energy auroras are shown to produce NO at increasingly lower altitudes. *Barth* [1992] shows calculations of NO abundance that are comparable to the 5 keV characteristic energy case of Figure 6. The peak NO abundances from the two calculations are in very good agreement.

[42] As stated earlier, the solar soft X-ray irradiance is entered into the glow model in 3 wavelength bands, 2–7 nm, 7–17 nm, and 17–20 nm. Figure 7 shows the relative

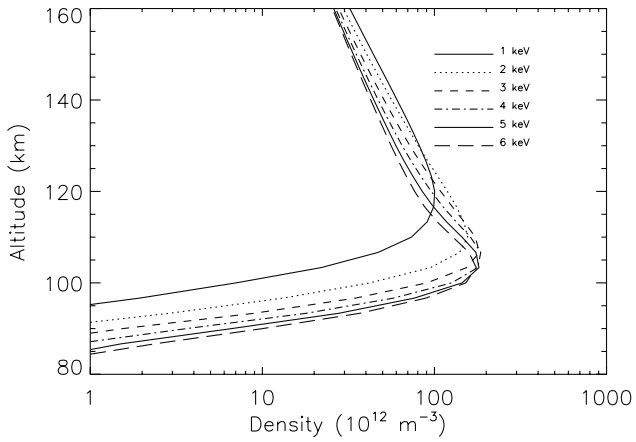

Figure 6. Nitric oxide densities as a function of altitude produced by auroral electrons of different characteristic energies as calculated by the steady state model. Geophysical conditions and energetic inputs are the same as in Figures 2 and 4.

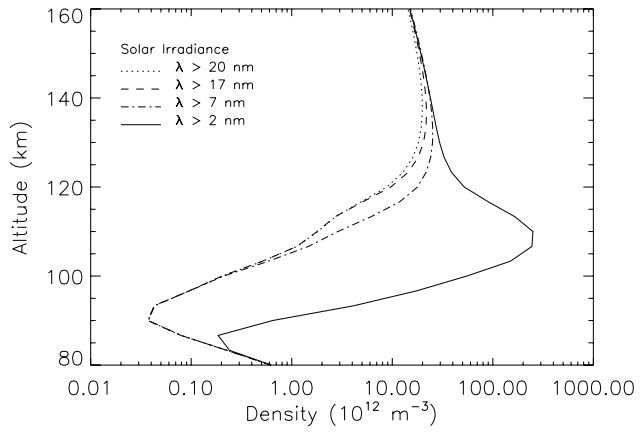

Figure 7. Nitric oxide densities as a function of altitude produced by solar irradiance as calculated by the steady state model. Geophysical conditions are the same as Figures 1 and 3. Shown are cases where only solar irradiance greater than 20 nm, greater than 17 nm, greater than 7 nm, and greater than 2 nm is considered.

importance of the three wavelength bands for the production of NO. Figure 7 shows 4 calculations of the NO abundance as a function of altitude as calculated by the steady state model using inputs from the glow model. In the first of the 4 models runs, only solar irradiance greater than 20 nm is considered. In the second case, 1 mW m^{-2} integrated energy flux in the 17–20 nm is considered as well and no energy in the shorter wavelength bands is considered. In the third case, 1 mW m^{-2} integrated energy flux in the 7–17 nm band is now included. Finally, in the fourth case, 1 mW m^{-2} integrated energy flux in the 2–7 nm band is included. Energy in the 7–17 nm and 17–20 nm wavelength ranges provide only small increases in the abundance of NO. It is the inclusion of the 2–7 nm irradiance that has a dramatic effect on the production of NO and leads to the peak in NO abundance near 106 km. *Swaminathan et al.* [2002] reached a similar conclusion.

5. Time-Dependent Calculation of Nitric Oxide Densities

[43] The model just described assumes geophysical conditions and energetic inputs to the atmosphere are constant in time. As discussed earlier, the NO abundance at any one time is indicative of the conditions over the past day; thus, a proper treatment of NO must take into account the varying geophysical conditions and energetic inputs. Time-dependent modeling of NO was first performed by *Gerard and Barth* [1977]. *Siskind et al.* [1990, 1995] and *Swaminathan et al.* [1998] have also presented one-dimensional time-dependent models of NO. The model presented here is new in that it includes an energetic electron transport calculation (glow) at each time step. In the time-dependent mode, the NOx model above is run just as before; however, whereas before all conditions were held constant until convergence was found, now conditions are allowed to change. The variation of the solar zenith angle throughout the day is accounted for; thus, the neutral atmosphere is allowed to vary as well as the photoioinization and photoelectron fluxes. This means that the MSIS model and the photoelectron calculation are utilized more heavily for this calculation. Typically time steps of one hour are utilized; however, experience has shown that near sunrise and sunset, smaller time steps on the order of 15 min are required. For the time-dependent case, an initial profile is required. Typically, the steady state solution is used. Experience has shown that the model reaches convergence after a period of five days. Here convergence implies that the results for a fifth day are not different from the results for a sixth day or in other words the diurnal variability is repeated.

[44] Figure 8 shows the results of the time-dependent solution for the low latitude solar irradiance (photoelectron) controlled case on day 266 of 1999. The latitude is 0°. A similar calculation for other time periods during the year (with the same energetic inputs) would yield only slightly different results depending on the solar zenith angle during that time period. Shown is the variation in NO and the photoelectron produced ionization rate of N_2 over the 24 hour time period at 106 km. The ionization begins at sunrise and progresses to a peak at local noon when the Sun is at zenith. After noon, the ionization rate decreases toward zero at sunset. Beginning at midnight, the NO is seen to be slowly increasing. This is due to NO being transported downward from above. As the Sun begins to rise, the NO abundance begins to decrease. The photodissociating solar irradiance is optically thin in the upper atmosphere and thus has an immediate effect. The photoionizing solar irradiance is optically thick in the upper atmosphere and thus does not begin to produce significant photoelectrons at 106 km until later. As the production of photoelectrons does begin to become significant, at around 10:00 local time, the NO abundance reaches a minimum and then begins to increase. The increase continues until about 17:00 local time when photodissociation again begins to dominate over photoelectron production. After sunset, when the atomic nitrogen and ionized molecular oxygen are mostly depleted, the slow nighttime increase due to transport begins again. Although the magnitude of the NO density changes throughout the year, the general characteristics of the diurnal variability of NO for low latitudes is similar to that shown in Figure 8 for each season.

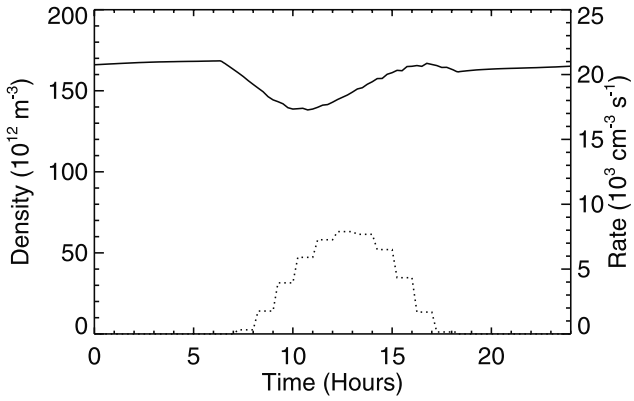

Figure 8. Nitric oxide densities (solid line) at 106 km as a function of time calculated by the time-dependent NO model using solar irradiance photoelectrons. The calculation is appropriate to 0° latitude and 0° longitude for day 266 of 1999 and uses a 2–7 nm solar irradiance of 1 mW m^{-2}. Shown are the last 48 hours of the model run. Also shown by the dotted line is the N_2 ionization rate at 106 km.

[45] Note that the magnitude of the NO abundance in Figure 8 is smaller by about 35% than the NO abundance at 106 km for the comparable 1 mW m^{-2} case of Figure 5. The steady state calculation, which assumes a constant energy flux, produces more NO than the time-dependent case which takes into account the varying energy input as the solar zenith angle varies. The NO abundance at any one time is sensitive to the magnitude of the energy input over the entire previous day. Steady state calculations are not appropriate for calculating NO abundances.

[46] Figure 9 shows the time dependant calculation for auroral cases. At auroral latitudes, the length of day varies strongly throughout the year, thus we show the time-dependent calculation at both equinoxes and both solstices. For each of these runs, the aurora is turned on for a full four days during the calculation and turned off at midnight at the beginning of the 5th day. The aurora has a constant energy flux of 1 mW m^{-2} and a characteristic energy of 4 keV. A value of 4 keV is typical for auroral characteristic energy. No solar soft X-ray irradiance is incorporated. The latitude is 65°.

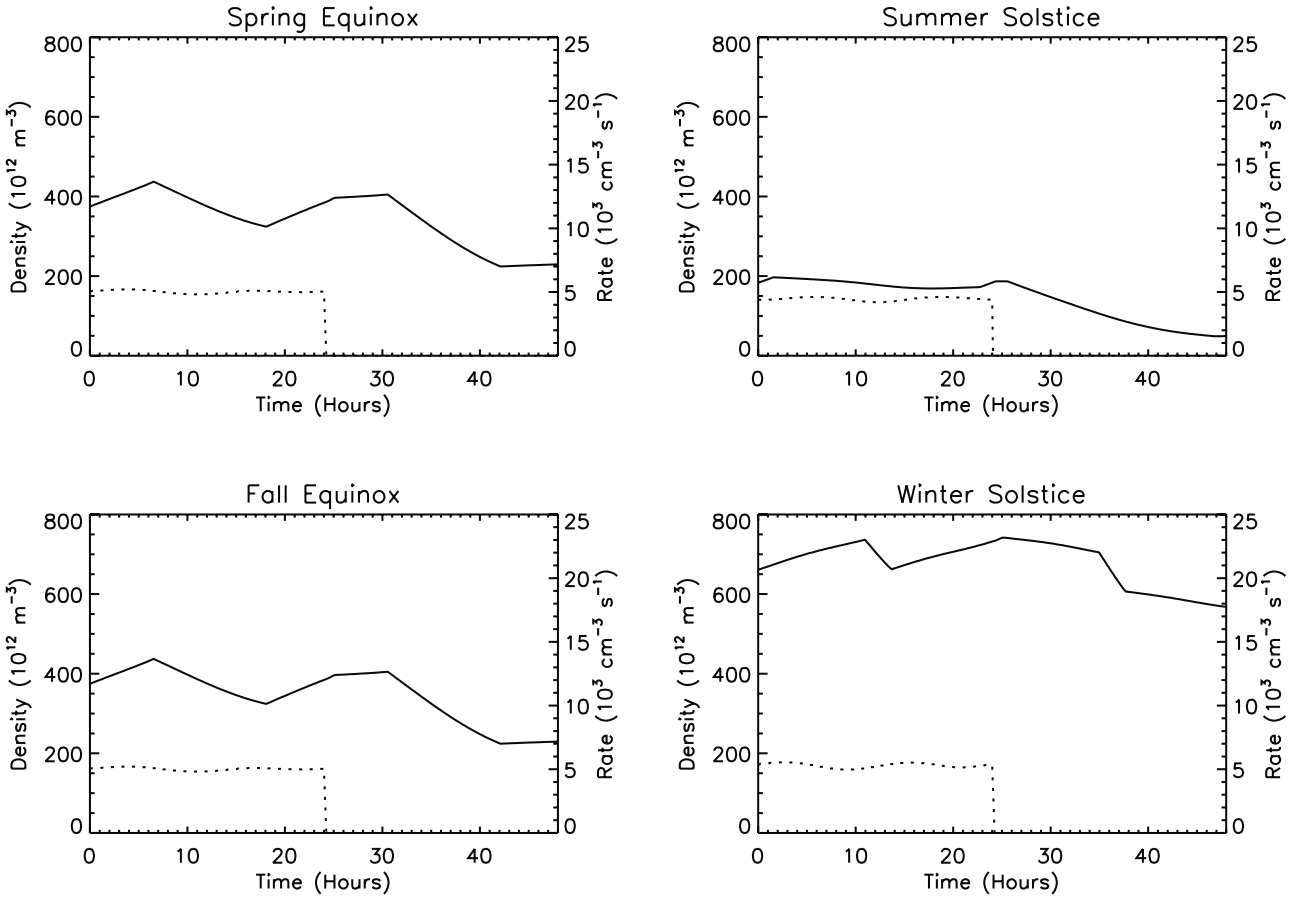

Figure 9. Nitric oxide densities (solid lines) at 106 km as a function of time calculated by the time-dependent NO model for auroral electrons. The calculation is appropriate to 65°N latitude and 0° longitude for four different days of 1999 and uses an auroral integrated energy flux of 1 mW m^{-2} and characteristic energy of 4 keV. Shown are the last 48 hours of the model run. Also shown by the dotted lines are the N_2 ionization rates at 106 km.

[47] The equinox cases show that while the aurora is occurring during the night, the NO abundance is increasing. When the Sun rises, photodissociation of NO begins to compete with auroral production of NO and in this case, photodissociation dominates and the NO density decreases. This continues until sunset when the NO begins to rise again. After midnight, when the aurora is no longer occurring, there is a slow increase due to transport from above but the increase is slower than when the aurora was present. During the daylight, there is no energy source and thus photodissociation causes the NO abundance to decrease. At sunset, the NO density will no longer increase.

[48] During the summer solstice, the same trends occur but the day is now nearly 24 hours long. While the aurora is occurring, auroral production of NO is competing with photodissociation of NO and the photodissociation wins with NO abundance decreasing throughout the day. When the aurora stops, there is no production of NO. The photodissociation of NO continues and the NO abundance therefore continues to decrease. The e-folding time constant of this decrease is as noted earlier, 0.8 days. Note that the overall NO abundance is always lower than for the equinox cases because of the photodissociation of NO that occurs throughout most of the day.

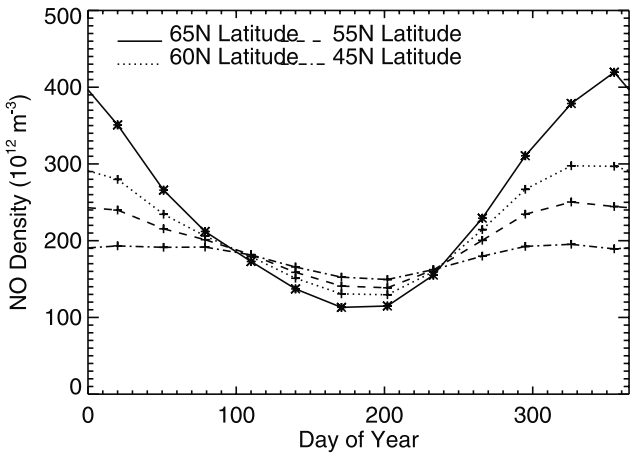

Figure 10. Nitric oxide densities (symbols) at 106 km and 11AM local time as a function of day of year calculated by the time-dependent NO model. The calculation is made at 4 latitudes and always 0° longitude. For each day, an auroral integrated energy flux of 1 mW m^{-2} and characteristic energy of 4 keV is assumed.

[49] For the winter solstice, the day is now extremely short. The nights are now so long that there is no significant photodissociation and large amounts of NO are allowed to build up as long as the aurora is occurring. In the lower right panel of Figure 9, a short decrease can be seen during the very short daytime (about 2 hours) at 65°N. After the aurora, the abundance declines slowly because there has also been large production of $N(^4S)$ and O_2^+. Again, the short day briefly enhances the decrease due to photodissociation of NO.

[50] Clearly, the length of day is an important factor in understanding the abundance of NO observed at any particular time. It is then useful to look at the seasonal behavior of NO for various latitudes. The magnitude and time dependence of NO is significantly different between the summer solstice, winter solstice, and equinox conditions. This point is highlighted in Figure 10 where the NO at 106 km is plotted as a function of day of year for four latitudes. In each case, as in Figure 9 the aurora has been turned on for 24 hours and turned off at the previous midnight. The values are for NO at 11AM local time (11 hours after the aurora ends), which is chosen since it is the local time of the SNOE measurements. The aurora for each day has an integrated energy flux of 0.5 mW m^{-2} and a characteristic energy of 4 keV. This figure shows that for the same auroral conditions, a measurement of NO abundance can be very different depending on the day of the year and the latitude. At each of the four latitudes shown, there is a minimum in NO at the summer solstice and a peak near the winter solstice. The reason for this is as described above, that the length of day, and therefore the role of photodissociation of NO, varies throughout the year. During the long summer day, photodissociation of NO limits the abundance of NO. During the short winter day, photodissociation of NO is much less effective and the NO abundance is able to accumulate to a larger amount. At 65°N, there is a factor of four variation over the year. By 60°N, the effect is reduced to approximately a factor of two, and by 45°N the effect is approximately 30% over the year. Clearly the day length is very important in relating NO measurements to energy flux.

6. Discussion

[51] We have developed a comprehensive one-dimensional model for the calculation of NO abundances as a function of geophysical conditions and energy input to the upper atmosphere. This model can be used to quantify the relationship between solar energetic inputs and NO abundance. Figure 11 shows that relationship for one particular case. In Figure 11, modeled NO abundances at 106 km for day 266 of 1999 are plotted as a function of solar energetic input fluxes. The lower curve is for 0° latitude at a local time of 11AM and NO is created by photoelectrons only. In this case the x axis represents the solar soft X-ray energy flux in the 2–7 nm spectral range. Over the known range of solar soft X-ray energy fluxes [*Bailey et al.*, 2000], the NO density varies linearly. The upper curve of Figure 11 is for the auroral case. Calculations are made for 65° latitude and

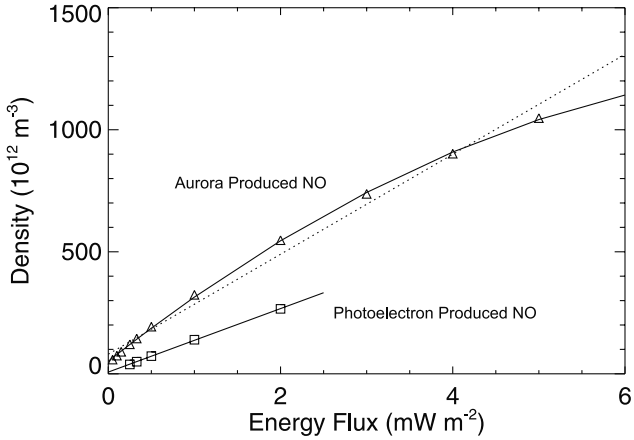

Figure 11. Nitric oxide densities (symbols) at 106 km at 11AM local time as a function of energy flux calculated by the time-dependent NO model. The solid line with squares is for the solar irradiance photoelectron case and the x axis represents the integrated 2 to 7 nm irradiance. The solid line is a linear fit to the model results (squares). The solid line with triangles is for the auroral case and assumes a characteristic energy of 4 keV. The x axis represents the integrated energy flux. In the auroral case, the model was run similarly to the previous auroral cases where the aurora was turned off at midnight prior to the observation. The calculations are made at 65° latitude and 0° longitude. The solid line is a parabolic fit to the model results (squares). The dotted line is a linear fit through the model results and shows that the relationship between auroral energetic input and NO abundance may be nonlinear.

Table A1. Updated Chemical Reaction Rates

Reaction	Rate Coefficient, cm^3 s^{-1}	Source
$NO + h\nu \rightarrow O + N(^4S)$	$J_\infty = 4.5 \times 10^{-6}$ s^{-1}	*Minschwaner and Siskind* [1993]
$O + e^* \rightarrow O^+ + 2e^-$		*Solomon et al.* [1988][a]
$O_2 + e^* \rightarrow O_2^+ + 2e^-$		*Solomon et al.* [1988][a]
$N_2 + e^* \rightarrow N_2^+ + 2e^-$		*Solomon et al.* [1988][a]
$N_2^+ + O \rightarrow NO^+ + N(^2D)$	$1.4 \times 10^{-10}\ (300/T)^{0.44}$	*McFarland et al.* [1974]
$N_2^+ + e^- \rightarrow N(^2D) + N(^4S) + e^-$	$1.8 \times 10^{-7}\ (T_e/300)^{-0.39}$	*Mehr and Biondi* [1969]
$O_2^+ + NO \rightarrow NO^+ + O_2$	4.4×10^{-10}	*Lindinger et al.* [1974]
$NO^+ + e^- \rightarrow O + N(^2D), N(^4S)$	$4.2 \times 10^{-7}\ (300/T_e)^{0.85}$ $f(N(^2D)) = 0.85$	*Torr et al.* [1976] and *Vejby-Christensen et al.* [1998]
$N(^4S) + O_2 \rightarrow NO + O$	$4.4\times 10^{-12} \exp(-3220/T)$	*Clark and Wayne* [1970]
$N(^2D) + O_2 \rightarrow NO + O$	6.0×10^{-12}	*Lin and Kaufman* [1971]
$N(^2D) + O \rightarrow N(^4S) + O$	6.9×10^{-13}	*Fell et al.* [1990]
$N(^4S) + NO \rightarrow N_2 + O$	3.4×10^{-11}	*Lee et al.* [1978]

[a] See also section 3.

assume a constant 4 keV aurora. The aurora, as in Figure 10, was held constant throughout the calculation until midnight of the last day. Results are shown for 11AM local time. The x axis represents the integrated auroral energy flux. The typical range of integrated energy fluxes for the aurora is much greater than for the soft X-ray irradiances. In the auroral case, the relationship between energy flux and NO density is nonlinear.

[52] *Barth et al.* [2001] show SNOE NO measurements at 106 km averaged around the period of day 266 1999. The measurements are averaged over many days in order to be representative of average auroral conditions. They show an NO abundance of about 300×10^{12} m^{-3}. For the assumptions of Figure 11, this abundance of NO would imply an average auroral energy flux of 0.65 mW m^{-2}. This value is not unreasonable. In an upcoming paper we will perform detailed comparisons between the predictions of the model described in this paper and the SNOE observations.

[53] Figure 11 shows a direct relationship between energy input and NO abundance. For the conditions used in the model runs that produced Figure 11, one could use an NO abundance to infer the energy deposited over the previous days. It must be kept in mind however that relationships such as shown in Figure 11 vary with local time of observation and throughout the year as discussed above and shown in Figures 8–10. The conclusion is that the observed NO abundance is directly related to the daily average energy input; but, the local time, day of year of the observation, and the behavior of the aurora over the previous day must be taken into account.

7. Conclusions

[54] A numerical model has been developed for the calculation of NO abundance as a function of altitude. The model is time-dependent and appropriate to any location or geophysical conditions. The glow energetic electron flux model is used to calculate the transport and flux of energetic electrons. A photochemical model that includes 35 chemical reactions and vertical diffusion is linked with the energetic electron flux calculation to produce a comprehensive model. It is shown that the time-dependence must be taken into account in calculating NO abundances and that a steady state assumption is inappropriate. It is further shown that the NO abundance is directly related to the amount of energy (solar irradiance or auroral) that has been deposited over the previous day; however, the exact relationship between energy input and NO abundance varies with local time and day of year. The model described here will be used to analyze NO observations from the SNOE mission.

Appendix A: Chemical Reaction Rates

[55] As stated in section 4, there are 35 reactions that are incorporated into the NO calculation. The full list of reactions and their rate coefficients is tabulated by *Barth* [1992]. Reaction rate coefficients are tabulated in Table A1 for all of the reactions discussed in this text as well as for the reactions for which the rate coefficients been updated since *Barth* [1992]. Included are the reaction, the relevant rate coefficient and the source for that rate coefficient.

[56] **Acknowledgments.** The authors would like to thank Phil Richards and the referees for helpful comments.

[57] Janet G. Luhmann thanks the referees for their assistance in evaluating this paper.

References

Avakyan, S. V., M. N. Vlasov, and I. A. Krinberg, Comparisons of the fluxes and spectra of auger electrons and photoelectrons in the Earth's ionosphere and plasmasphere, *Geomagn. Aeron.*, *17*, 54, 1977.

Bailey, S. M., T. N. Woods, C. A. Barth, and S. C. Solomon, Measurements of the solar soft X-ray irradiance from the Student Nitric Oxide Explorer, *Geophys. Res. Lett.*, *26*, 1255, 1999.

Bailey, S. M., T. N. Woods, C. A. Barth, S. C. Solomon, R. Korde, and L. R. Canfield, Measurements of the solar soft X-ray irradiance by the Student Nitric Oxide Explorer: First analysis and underflight calibrations, *J. Geophys. Res.*, *105*, 27,179, 2000.

Bailey, S. M., T. N. Woods, C. A. Barth, S. C. Solomon, R. Korde, and L. R. Canfield, Correction to "Measurements of the solar soft X-ray irradiance by the Student Nitric Oxide Explorer: First analysis and underflight calibrations, *J. Geophys. Res.*, *106*, 15,791, 2001.

Barth, C. A., Planetary ultraviolet spectroscopy, *Appl. Opt.*, *8*, 1295, 1969.

Barth, C. A., Nitric oxide in the lower thermosphere, *Planet. Space Sci.*, *40*, 315, 1992.

Barth, C. A., W. K. Tobiska, D. E. Siskind, and D. D. Cleary, Solar-terrestrial coupling: Low-latitude thermospheric nitric oxide, *Geophys. Res. Lett.*, *15*, 92, 1988.

Barth, C. A., S. M. Bailey, and S. C. Solomon, Measurements of thermospheric nitric oxide from the Student Nitric Oxide Explorer, *Geophys. Res. Lett.*, *26*, 1251, 1999.

Barth, C. A., D. N. Baker, K. D. Mankoff, and S. M. Bailey, The northern auroral region as observed in nitric oxide, *Geophys. Res. Lett.*, *28*, 1463, 2001.

Belitza, D., International reference ionosphere: Recent developments, *Radio Sci.*, *21*, 343, 1986.

Berkowitz, J., *Photoabsorption, Photoionization, and Photoelectron Spectroscopy*, Academic, San Diego, Calif., 1979.

Cicerone, R. J., and S. A. Bowhill, Photoelectron fluxes in the ionosphere computed by a Monte Carlo method, *J. Geophys. Res.*, *76*, 8299, 1971.

Cicerone, R. J., W. E. Swartz, R. S. Stolarski, A. F. Nagy, and J. S. Nisbet, Thermalization and transport of photoelectrons: A comparison of theoretical approaches, *J. Geophys. Res.*, *78*, 6709, 1973.

Clark, I. D., and R. P. Wayne, Kinetics of the reaction between atomic nitrogen and molecular oxygen in the ground ($^3\Sigma_g^-$) and the first excited ($^1\Delta_g$) states, *Proc. R. Soc. London, Ser. A*, *A316*, 359, 1970.

Cleary, D. D., Daytime high-latitude rocket observations of the NO γ, δ, and ε bands, *J. Geophys. Res.*, *91*, 11,337, 1986.

Colegrove, F. D., W. B. Hanson, and F. S. Johnson, Eddy diffusion and oxygen transport in the lower thermosphere, *J. Geophys. Res.*, *70*, 4931, 1965.

Conway, R. R., Photoabsorption and photoionization cross sections of O, O2, and N2 for photoelectron production calculations: A compilation of recent laboratory measurements, *NRL Memo. Rep. 6155*, Nav. Res. Lab., Washington, D.C., 1988.

Dalgarno, A., M. B. McElroy, and R. J. Moffeitt, Electron temperatures in the ionosphere, *Planet. Space Sci.*, *11*, 463, 1963.

Dalgarno, A., M. B. McElroy, and A. I. F. Stewart, Electron impact excitation of the dayglow, *J. Atmos. Sci.*, *26*, 753, 1969.

Eparvier, F. G., Nitric oxide in the lower thermosphere, Ph.D. thesis, Univ. of Colorado, Boulder, Colo., 1991.

Fell, C., J. I. Steinfield, and S. Miller, Quenching of N(^{2}D) by O (^{3}P), *J. Chem. Phys.*, *92*, 4768, 1990.

Fennelly, J. A., and D. G. Torr, Photoionization and photoabsorption cross sections of O, N_2, O_2, and N for aeronomic calculations, *At. Data and Nucl. Data Tables*, *51*, 321, 1992.

Gerard, J.-C., and C. A. Barth, High-latitude nitric oxide in the lower thermosphere, *J. Geophys. Res.*, *82*, 674, 1977.

Green, A. E. S., and C. A. Barth, Calculations of the photoelectron excitation of the dayglow, *J. Geophys. Res.*, *72*, 3975, 1967.

Hanson, W. B., and F. S. Johnson, Electron temperatures in the ionosphere, *Mem. Soc. R. Sci. Liege*, *5*, 390, 1961.

Hedin, A. E., MSIS-86 thermospheric model, *J. Geophys. Res.*, *92*, 4649, 1987.

Hinteregger, H. E., K. Fukui, and G. R. Gilson, Observational, reference, and model data on solar EUV, from measurements on AE-E, *Geophys. Res. Lett.*, *8*, 1147, 1981.

Lee, J. H., J. V. Michael, W. A. Payne, and L. J. Stief, Absolute rate of the reaction of N(^{4}S) with NO from 196°–400°K with DF-RF and FP-RF techniques, *J. Chem. Phys.*, *69*, 3069, 1978.

Lin, C. L., and F. Kaufman, Reactions of metastable nitrogen atoms, *J. Chem. Phys.*, *55*, 3760, 1971.

Lindinger, W., F. C. Fehsenfeld, A. L. Schmeltekopf, and E. E. Ferguson, Temperature dependence of some ionospheric ion-neutral reactions from 300°–900°K, *J. Geophys. Res.*, *79*, 4753, 1974.

Link, R., Dayside magnetospheric cleft auroral processes, Ph.D. thesis, York Univ., Toronto, Ont., Canada, 1982.

Link, R., Feautrier solution of the electron transport equation, *J. Geophys. Res.*, *97*, 159, 1992.

McFarland, M., D. L. Albritton, F. C. Fehsenfeld, E. E. Ferguson, and A. L. Schmeltekopf, Energy dependence and branching ratio of the $N_2^+ + O$ reaction, *J. Geophys. Res.*, *79*, 2925, 1974.

Mehr, F. J., and M. A. Biondi, Electron temperature dependence of recombination of O_2^+ and N_2^+ ions with electrons, *Phys. Rev.*, *181*, 264, 1969.

Minschwaner, K., and D. E. Siskind, A new calculation of nitric oxide photolysis in the stratosphere, mesosphere, and lower thermosphere, *J. Geophys. Res.*, *98*, 20,401, 1993.

Nagy, A. F., and P. M. Banks, Photoelectron fluxes in the ionosphere, *J. Geophys. Res.*, *75*, 6260, 1970.

Oran, E. S., and D. J. Strickland, Photoelectron flux in the Earth's ionosphere, *Planet. Space Sci.*, *26*, 1161, 1978.

Richards, P. G., and D. G. Torr, Auroral modeling of the 3371 Å auroral emission rate: Dependence on characteristic electron energy, *J. Geophys. Res.*, *95*, 10,337, 1990.

Rusch, D. W., and C. A. Barth, Satellite measurements of nitric oxide in the polar regions, *J. Geophys. Res.*, *80*, 3719, 1975.

Russell, J. M., III, L. L. Gordley, J. H. Park, S. R. Drayson, D. H. Hesketh, R. J. Cicerone, A. F. Tuck, J. E. Frederick, J. E. Harries, and P. J. Crutzen, The halogen occultation experiment, *J. Geophys. Res.*, *98*, 10,777, 1993.

Siskind, D. E., C. A. Barth, and R. G. Roble, The response of thermospheric nitric oxide to an auroral storm, 1, Low and middle latitudes, *J. Geophys. Res.*, *94*, 16,885, 1989a.

Siskind, D. E., C. A. Barth, D. S. Evans, and R. G. Roble, The response of thermospheric nitric oxide to an auroral storm, 2, Auroral latitudes, *J. Geophys. Res.*, *94*, 16,899, 1989b.

Siskind, D. E., C. A. Barth, and D. D. Cleary, The possible effect of solar soft X rays on thermospheric nitric oxide, *J. Geophys. Res.*, *95*, 4311, 1990.

Siskind, D. E., D. J. Strickland, R. R. Meier, T. Majeed, and F. G. Eparvier, On the relationship between the solar soft X-ray flux and thermospheric nitric oxide: An update with an improved photochemical model, *J. Geophys. Res.*, *100*, 19,687, 1995.

Solomon, S. C., and V. J. Abreu, The 630-nm dayglow, *J. Geophys. Res.*, *94*, 6817, 1989.

Solomon, S. C., P. B. Hays, and V. J. Abreu, The auroral 6300 Å emission: Observations and modeling, *J. Geophys. Res.*, *93*, 9867, 1988.

Solomon, S. C., C. A. Barth, and S. M. Bailey, Auroral production of nitric oxide measured by the Student Nitric Oxide Explorer, *Geophys. Res. Lett.*, *26*, 1259, 1999.

Solomon, S. C., S. M. Bailey, and T. N. Woods, Effect of solar soft X rays in the lower ionosphere, *Geophys, Res. Lett.*, *28*, 2149, 2001.

Stamnes, K., On the two stream approach to electron transport and thermalization, *J. Geophys. Res.*, *86*, 2405, 1981a.

Stamnes, K., Electron transport and energy degradation: On the numerical solution to the two-stream equations, *Sci. Rep. UAG R-286*, Geophys. Inst., Univ. of Alaska, Fairbanks, Fairbanks, 1981b.

Stewart, A. I. F., Photoionization coefficients and photoelectron impact excitation efficiencies in the daytime ionosphere, *J. Geophys. Res.*, *75*, 6333, 1970.

Strickland, D. J., D. L. Book, T. P. Coffey, and J. A. Fedder, Transport equation techniques for the deposition of auroral electrons, *J. Geophys. Res.*, *81*, 2755, 1976.

Strickland, D. J., and R. R. Meier, A photoelectron model for the rapid calculation of atmospheric excitation rates, *NRL Memo. Rep. 5004*, Nav. Res. Lab., Washington, D.C., 1982.

Swaminathan, P. K., et al., Nitric oxide abundance in the mesosphere/lower thermosphere region: Roles of solar soft x rays, suprathermal N (4S) atoms, and vertical transport, *J. Geophys. Res.*, *103*, 11,579, 1998.

Swaminathan, P. K., D. F. Strobel, L. Acton, and L. J. Paxton, Model update for mesospheric/thermosphere nitric oxide, *Phys. Chem. Earth*, in press, 2002.

Tobiska, W. K., Revised solar extreme ultraviolet flux model, *J. Atmos. Terr. Phys.*, *53*, 1005, 1991.

Torr, D. G., M. R. Torr, J. C. G. Walker, L. H. Brace, H. C. Britton, W. B. Hansen, J. H. Hoffman, A. D. Nier, and M. Oppenheimer, Recombination of NO^+ in the ionosphere, *Geophys. Res. Lett.*, *3*, 209, 1976.

Vejby-Christensen, L., D. Kella, H. B. Pedersen, and L. H. Anderson, Dissociative recombination of NO^+, *Phys. Rev. A*, *57*, 3627, 1998.

Von Rosenberg, D. U., *Methods for Numerical Solution of Partial Differential Equations*, Elsevier Sci., New York, 1969.

Winningham, J. D., D. T. Decker, J. U. Kozyra, J. R. Jasperse, and A. F. Nagy, Energetic (>60 eV) atmospheric photoelectrons, *J. Geophys. Res.*, *94*, 15,225, 1989.

Woods, T. N., and G. J. Rottman, Solar EUV irradiance derived from a sounding rocket experiment on November 10, 1988, *J. Geophys. Res.*, *95*, 6227, 1990.

S. M. Bailey, Geophysical Institute, University of Alaska, P.O. Box 757320, Fairbanks, AK 49775-7320, USA. (scott.bailey@gi.alaska.edu)

C. A. Barth, Laboratory for Atmospheric and Space Physics, University of Colorado, 3450 Mitchell Lane, Boulder, CO 80301, USA. (charles.barth@lasp.colorado.edu)

S. C. Solomon, High Altitude Observatory, National Center for Atmospheric Research, 1850 Table Mesa Drive, Boulder, CO 80305, USA. (stans@ucar.edu)